Climate Dynamics manuscript No.
(will be inserted by the editor)

Mixed precipitation occurrences over southern Québec, Canada, under warmer climate conditions using a Regional Climate Model.

Dominic Matte · Julie M. Thériault · René Laprise

Received: date / Accepted: date

Abstract Winter weather events with temperatures near 0°C are often associated with freezing rain. They can have major impacts on the society by causing power outages and disruptions to the transportation networks. Despite the catastrophic consequences of freezing rain, very few studies have investigated how their occurrences could evolve under climate change. This study aims to investigate the change of freezing rain and ice pellets over southern Québec using regional climate modeling at high resolution. The fifth-generation Canadian Regional Climate Model with climate scenario RCP 8.5 at 0.11° grid mesh was used. The precipitation types such as freezing rain, ice pellets or their combination are diagnosed using 5 methods (Cantin and Bachand, Bourgouin, Ramer, Czys and, Baldwin). The occurrences of the diagnosed precipitation types for the recent past (1980-2009) are found to be comparable to observations. The projections for the future scenario (2070-2099) suggested a general decrease in

D. Matte (✉) · René Laprise · Julie M. Thériault

Centre ESCER, Department of Earth and Atmospheric science, Université du Québec à Montréal (UQAM), P.O. Box 8888, Downtown Station, Montréal, QC, Canada, H3C 3P8.

Tel.: 1-514-987-3000 ext 2194, Fax: 1-514-987-7749

E-mail: mattedominic3@gmail.com

the occurrences of mixed precipitation over southern Québec from October to April. This is mainly due to a decrease in long-duration events (≥6h). Overall, this study contributes to better understand how the distribution of freezing rain and ice pellets might change in the future using high-resolution regional climate model.

Keywords Climate change · High-resolution climate simulation · Multiple nesting · Freezing Rain · Ice pellet · Precipitation-type algorithm

1 Introduction

In winter, the passage of warm fronts in mid-latitude regions can lead to a typical vertical temperature structure composed of a warm air layer (T>0°C) overlaying a cold-air layer (T<0°C) near the surface. Such vertical temperature structure may produce freezing rain, ice pellets or their combination (Cortinas, 2000; Cortinas Jr et al., 2004; Groisman et al., 2016). Some regions are particularly prone to such precipitation types, such as near St. Johns, Newfoundland, as well as mountainous areas of northeastern North America. For example, the US Appalachian region (Rackley and Knox, 2016) is often influenced by the phenomena of cold air damming that could lead to freezing precipitation. Furthermore, the St. Lawrence River Valley (SLRV) is also prone to freezing precipitation because of wind channeling effects (Carrera et al., 2009).

Cortinas (2000) conducted a freezing rain climatology in the Great Lakes region in North America. He stated that storm track, the proximity of the Atlantic Ocean, the lakes and the topography create a large spatial and temporal variability of freezing rain in that region. Cortinas Jr et al. (2004) extended this study on the occurrence of freezing precipitation, freezing drizzle and ice pellets between 1976 and 1990 to the continental United State and Canada. They showed that the highest frequency of freezing rain and ice pellets occurs in St. Johns area as well as in the SLRV, as confirmed by the studies of Stuart and Isaac (1999) and Groisman et al. (2016). The maximum reported in the SLRV is due to a combination of factors such as the relative location of the extratropical storm track, water source proximity and topographical features (Bernstein, 2000; Roebber and Gyakum, 2003; Cortinas Jr et al., 2004). Although topography is not considered a sufficient condition for freezing precipitation formation, many studies have mentioned its importance on producing the favorable near-surface conditions (Stuart and Isaac, 1999; Cortinas, 2000; Cortinas Jr et al., 2004; Henson et al., 2011). For example, the high frequency of freezing precipitation in the SLRV is related to wind channeling of cold air near the surface (Whiteman and Doran, 1993; Roebber and Gyakum, 2003).

The measurement and simulation of freezing rain and ice pellets is challenging because they are often composed of both liquid and solid, and they mainly occur at temperatures near 0°C. Two main approaches can be used to determine the precipitation types in atmospheric models. The first approach is diagnostic, which involves using the current state of the atmosphere by using variables such as the temperature and the relative humidity on different pressure levels (Reeves et al., 2014; Bourgouin, 2000; Baldwin and Contorno, 1993; Cantin and Bachand, 1993; Czys et al., 1996; Ramer, 1993). The second approach uses microphysics equations to predict the mass mixing ratio and number concentration of the different types of precipitation (Milbrandt and Yau, 2005a,b; Morrison and Grabowski, 2008; Morrison and Milbrandt, 2015). Although this approach is more physically based, it is computationally expensive.

It is thus more affordable to use diagnostic methods to conduct climate studies.

Few studies have been focusing on freezing rain in a context of climate change (Cheng et al., 2007, 2011; Lambert and Hansen, 2011; Klima and Morgan, 2015). Cheng et al. (2011) studied freezing rain occurrences over eastern Canada by statistically downscaling several general circulation models at the location of observing stations. They found a projected increase of freezing rain during the coldest months and a decrease during the transition seasons (fall and spring). Lambert and Hansen (2011) used a different approach. They post-processed the third-generation Canadian Coupled Climate Model to diagnose the future freezing rain occurrences. Their study suggested a poleward shift of the freezing precipitation, which is explained by the poleward shift of the 0°C isotherm. Nevertheless, they also mentioned that their coarse spatial and temporal resolutions were probably not sufficient to highlight key factors producing freezing rain. Finally, Klima and Morgan (2015) performed an idealized experiment using vertical historical temperature profiles on which they applied several warming scenarios to explore how freezing rain may change under these conditions. They also found a poleward shift of the freezing rain as well as an increase in winter rather than in the transition seasons.

High-resolution climate simulations are required for an adequate representation of local topography and key processes leading to freezing and frozen precipitation formation (Lucas-Picher et al., 2016). These would be, however, very expensive to run with Global Circulation models (GCMs). The use of nested limited-area Regional Climate Models (RCMs) to dynamically downscale GCM simulations allows drastically reducing the computational cost while benefiting from the value added by an increased of resolution. At very high spatial resolution, the computational cost of RCM can be further reduced using multiple dynamical downscaling (e.g., Cholette et al., 2015; Matte et al., 2016). The study of Cholette et al. (2015) has shown that the wind channeling in the St. Lawrence River Valley is fairly well represented with a grid spacing of ≤ 9 km. Matte et al. (2016) have shown that multiple nesting was not only technically feasible but also appropriate, to some extent, to conduct high-resolution climate modeling.

The main goal is to conduct high-resolution regional climate simulations to study the evolution of freezing rain, ice pellets and their mixture (hereinafter referred as mixed precipitation) associated with climate change. The study focuses over the Québec Province during past (1980-2009) and projected future climate (2070-2099) under a Representative Concentration Pathway (RCP) 8.5 future scenario (Meinshausen et al., 2011). The RCP 8.5 was chosen to address the changes in mixed precipitation in warmest conditions.

This paper is organized as follows. The experimental design, a description of the regional climate model, its configurations and a brief description of the algorithms used to diagnose the precipitation types are presented in the next Section. The past simulated climate is discussed in Section 3 and the future simulated climate and its associated climate change is discussed in Section 4. Finally, the main results are summarized and discussed in Section 5.

2 Experimental design

2.1 CRCM5 configuration

The simulations have been performed with the fifth-generation Canadian Regional Climate model (CRCM5; see Hernández-Díaz et al., 2013, for a detailed description). The physical parameterization of the CRCM5 is mostly based on the 33-km meso-global Global Environmental Model (GEM, Bélair et al. 2005, 2009) employed for numerical weather prediction by the Canadian Meteorological Centre: Kain-Fritsch deep convection parameterization (Kain and Fritsch, 1990), Kuo-transient shallow convection (Kuo, 1965; Bélair et al., 2005), Sundqvist resolved-scale condensation (Sundqvist et al., 1989), correlated-K terrestrial and solar radiation schemes (Li and Barker, 2005), subgrid-scale orographic effects following the mountain gravity-wave drag of McFarlane (1987) and low-level orographic blocking scheme of Zadra et al. (2003) for the turbulent kinetic energy closure planetary boundary layer and vertical diffusion (Benoit et al., 1989; Delage and Girard, 1992; Delage, 1997). On the other hand CRCM5 uses the most recent version of the Canadian Land Surface Scheme (CLASS 3.5; Verseghy, 2000, 2008) that allows a detailed representation of vegetation, land-surface types, organic soil and a flexible number of ground layers, and lakes are represented by the 1-D FLake model (Martynov et al., 2012).

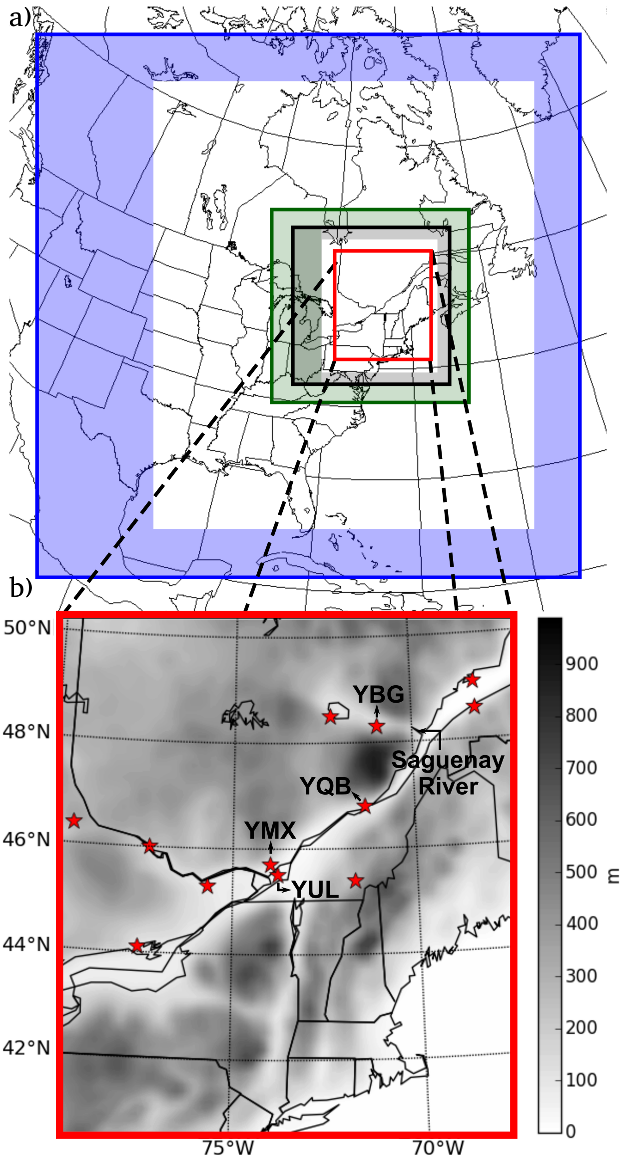

Fig. 1 The domain location for the different experimental setups. (a) shows the domain location of the intermediate-resolution simulation (in blue) and the high-resolution simulation (in black) used for the two-step dynamical downscaling of the historical and climate-change simulations. The green square is the domain location used for the hindcast simulation. The color shadings represent the spatial spin-up region for each case. The red square represents the "trustworthy" region of a size of 80 x 90 grid points. (b) is the topography (grey shading) and the location of the MANOBS stations (red stars). The stations labeled are Pierre-Elliot Trudeau airport (YUL), Mirabel (YMX), Québec City (YQB) and Bagotville (QBG)

2.2 Hindcast simulation setup

The domain for the hindcast simulation is shown by the green square in Fig.1a. The grid mesh is 0.11° and the domain contains 160 x 160 grid points (including the Davies sponge zone). The integration is performed with a time step of 300 s and 56 terrain-following levels in the vertical. The hindcast simulation (noted CRCM5/ERA) was driven by ERA40 reanalysis data from 1975 to 1978 and continued with ERA-Interim reanalysis data (ERA-I) for the period 1979 to 2009, on a 0.75° grid, at a 6-hourly interval. The study starts in 1980 to ensure enough time for spin up. The jump of resolution between the lateral boundary conditions and the RCM mesh is about 7; as suggested by the study of Matte et al. (2017), a lateral spin-up region should be taken into consideration to make sure that the fine-scale features can fully develop (Fig.1, green region). The analysis region centered on Montréal, Québec, Canada, encompasses 80 x 90 grid points (Fig.1a and b).

2.3 Historical and projected climate simulations setup

The Max-Planck Institute for Meteorology Earth System model (MPI-ESM-LR) with a linear transform grid of a 2.8°, is used as boundary conditions to drive the CRCM5. For computational cost considerations (Matte et al., 2016), the GCM-driven simulations have been realized using a two-step dynamical downscaling approach. In the first step a 0.45° grid mesh CRCM5 simulation is driven by MPI-ESM-LR, resulting in a jump of resolution of about 6, over a domain covering a 110 x 110 grid-point area (blue square in Fig.1a) with a time step of 20 min; this simulation is denoted as RCM45. In the second step, the RCM45 data is used to provide the lateral boundary conditions at hourly intervals to the CRCM5 on a 0.11° mesh, resulting in a jump of resolution of about 4, covering a 130 x 130 grid-point domain (black square in Fig.1a), with a time step of 300 s; this simulation is denoted CRCM5/MPI. The analysis domain is the same as that for the hindcast simulation; the CRCM5 domains for the two steps have been chosen to follow the optimal configuration suggested by the study of Matte et al. (2017), and the lateral spin-up regions are shown by the colored bands in Fig.1a. The quoted domain sizes include the Davies sponge zones.

Time slices are used to reduce the CRCM5 computing cost. The first stage periods are 1970-2009 and 2060-2099, and the second stage periods are 1975-2009 and 2065-2099, for the historical and projected climate simulations, respectively. This leaves 5 years between each step to ensure that the simulations had time to adjust correctly. The simulations after 2006 followed the RCP 8.5 scenario (Meinshausen et al., 2011).

2.4 Diagnostic of precipitation types

Five precipitation-type algorithms have been used to provide a range of estimates in the distribution of mixed precipitation at the surface. The study focuses on mixed precipitation, rather than freezing rain and ice pellets separately, to overcome issues about their distinction in both the algorithms and the observations (Reeves et al., 2014). Most calculations have been computed on model levels, except for the partial thickness method of Cantin and Bachand (1993). Short descriptions of the five algorithms are provided below.

The Bourgouin (2000) algorithm is based on calculating, in an aerological diagram, the positive and negative area (in J kg^{-1}). By comparing those two areas and using defined thresholds, precipitation types can be diagnosed as snow, ice pellets, freezing rain and rain. The thresholds have been defined by Bourgouin (2000) using a database of collocated surface precipitation observations and upper air sounding for two cold seasons (1989-90 and 1990-91) over North America. Mixed precipitation is defined when freezing rain or/and ice pellet are diagnosed. This scheme is already implemented in GEM for weather forecast, and it has been tested in CRCM5 on past climatology over the province of Québec and demonstrated good comparison with observations (Bresson et al., 2017).

The Czys approach (Czys et al., 1996) is a physically based algorithm using a non-dimensional parameter to distinguish freezing rain and ice pellets. The residence time of a 400-μm frozen hydrometeor falling in a warm layer is compared to its melting time. The onset melting temperature derives from the theory of Drake and Mason (1966), which is based on the rate of energy supplied by the environment to the particle and the rate of energy required to melt the frozen particle. The mixed precipitation is defined when freezing rain or ice pellets occurs.

The Ramer (1993) scheme is based on a calculation of the ice fraction using basic parameters such as the temperature, wet-bulb temperature and relative humidity. It differentiates among snow, ice pellets, mix of snow and rain, mix of freezing rain and ice pellets, snow, freezing rain and rain. The mixed precipitation with this method is defined when ice pellet, mix of freezing rain and ice pellets or freezing rain occurs.

The partial thickness method developed by Cantin and Bachand (1993) scheme (CB) compares the thickness of the 1000-850 hPa and the 850-700 hPa layers. Mixed precipitation is diagnosed when the precipitation falls within a 850-700 hPa layer with a thickness greater than 154 dam, followed by a 1000-850 hPa layer with a thickness less than 131 dam. An additional criterion, requiring that the 2-meter temperature be below freezing temperature has been added. This 2-meter temperature criterion is a necessary but not sufficient condition for mixed precipitation.

The method of Baldwin and Contorno (1993) diagnoses the precipitation level and then calculates diagnosed ice crystals if the temperature is below 269 K. Those ice crystals, then, evolve through different phases changes according to the wet-bulb temperature and the near-surface temperature. In this study, we have followed the modifications suggested by Cortinas et al. (2002), which use a similar decision tree but have modified the thresholds. Mixed precipitation with this method includes both ice pellets and freezing rain.

2.5 Available Observations

To evaluate the precipitation type diagnostic, observation data from the Environment and Climate Change Canada surface stations (MANOBS for Manual Observations) were used. The database provides hourly occurrences of the precipitation types. The observations were carefully quality-controlled. Only the stations with hourly observations were used. Also, the stations associated with missing data for more than a month over the study period were rejected, as well as other data that were not validated by the National Climate Archive. The stations retained in this study are shown in Fig.1b.

2.6 Methodology

As suggested by Lambert and Hansen (2011), a minimal threshold of 1 mm/day is applied to consider a precipitation event. An event is defined when mixed precipitation was diagnosed at the surface, as defined for each of the 5 algorithms in section 2.4. If less than 6 h without precipitation occurred between two mixed precipitation episodes, they are counted as a single event. For observations, mixed precipitation is defined when freezing rain or/and ice pellets were reported. The closest grid point associated with a similar topographic height is used to compare model results with a specific station. Appendix B is discussing the sensitivity of the chosen grid point. The next section evaluates the CRCM5 skills by comparing the observations with the CRCM5/ERA simulation. To evaluate the boundary forcing errors, Appendix A is showing the differences between CRCM5/MPI and CRCM5/ERA for the 1980-2009 period.

3 Past climatology of mixed precipitation

3.1 Occurrence of mixed precipitation

The mean annual number of hours of mixed precipitation at the stations (disks) and using the 5 algorithms in the CRCM5/ERA simulation are shown in Fig.2. All algorithms captured the main mixed-precipitation occurrence pattern, such as the maximum values over the Appalachian Mountains, the Charlevoix Mountains, the Laurentian Mountains, the Saguenay River, as well as a relative maximum near the SLRV area. Relatively higher number of hours of mixed precipitation is found at higher elevations where the surface temperature is often below 0°C during winter. The average of all five algorithms is shown in panel 2f. Unfortunately, it is difficult to confirm the numerical results as few observations are available in the area. Panel 2g displays the annual standard deviation calculated around the average value, showing a wider range of occurrences in complex terrain, confirming that the occurrence of mixed precipitation is sensitive to the topography.

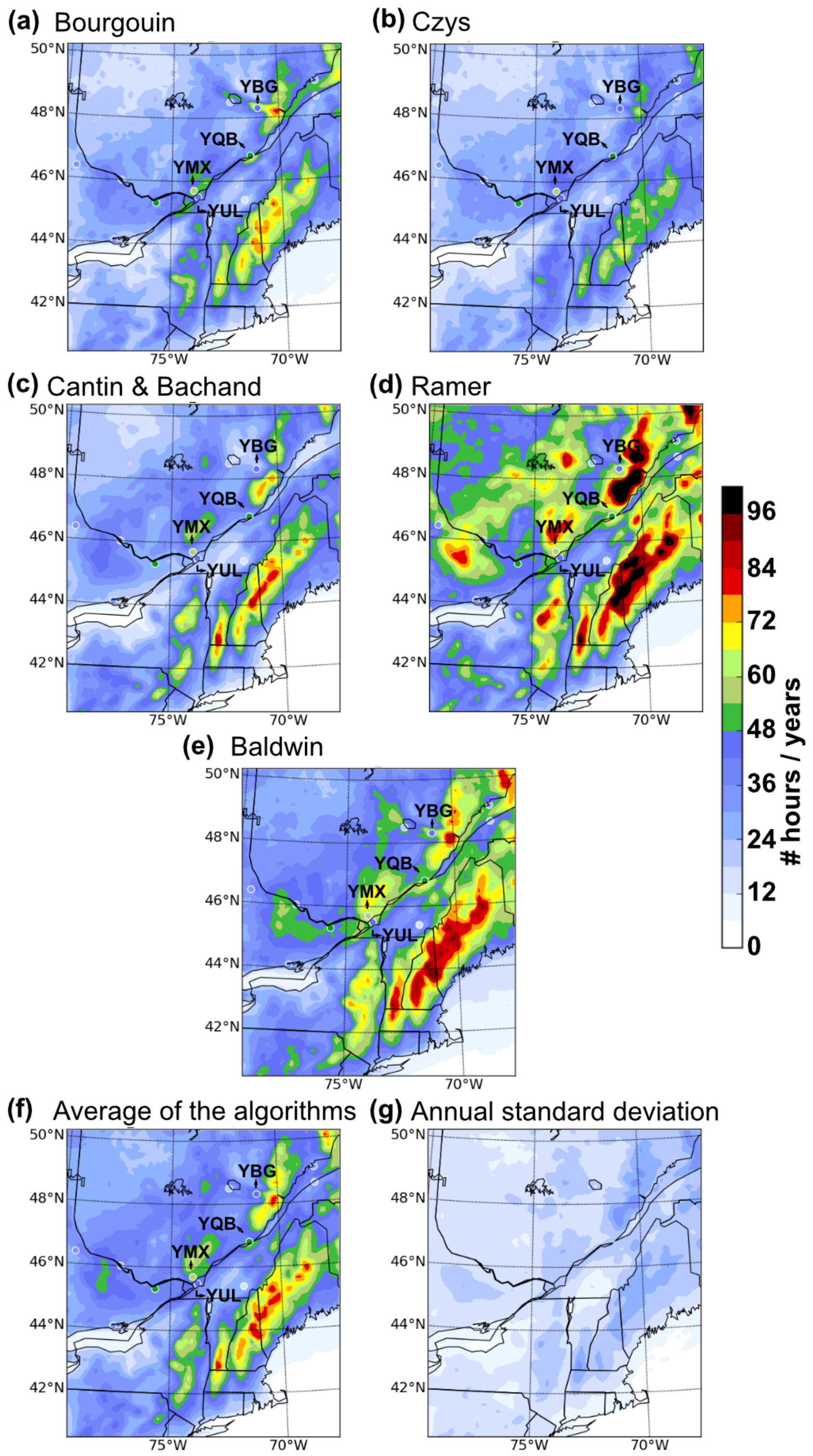

Fig. 2 Mean annual hourly occurrence of mixed precipitation diagnosed by a) Bourgouin, b) Czys, c) Cantin and Bachand, d) Ramer, e) Baldwin, f) the average among the 5 algorithms and g) the standard deviation around their average. The stations are indicated by the white circles and the values are the same as the color bar.

Figure 3 shows the mean annual hourly occurrence of mixed precipitation at 4 observation stations. To give an insight of the sensitivity of the selected grid point, the standard deviation of the nine nearest grid points of the MANOBS station is also indicated by the black lines for each algorithm. There are some differences and similarities among the results of the 5 algorithms. Although that the Bourgouin, the Czys, the Ramer and the Baldwin algorithms reproduce modestly well the observations at Mirabel (YMX), Montréal (YUL) and Québec City (YQB), substantial differences can be noted between the algorithms. The Czys algorithm produced an underestimation of mixed precipitation over the SLRV (see also Fig.2b), which could be due to the temperature at which the melting of the 400-μm frozen hydrometeor starts. The CB algorithm also underestimates mixed precipitation occurrences for all four stations (Fig.3). Since that CB compares two fairly large atmospheric layers, when the melting occurs within the 1000-850 hPa layer, this scheme did not capture it, and hence no mixed precipitation was diagnosed (not shown). This explains partly the underestimation of mixed precipitation for the CB show in Fig.2c. Although that the Ramer and the Baldwin algorithms reproduced well the number of hours of mixed precipitation for YUL and YMX, they overestimated it at YQB and YBG. Some areas are also associated with higher values. This is because the temperature threshold at the top of the precipitation layer diagnosed in Ramer (T_w=-6.6 °C) and Baldwin (T=-4°C) are colder than the other algorithms, allowing more supercooled liquid precipitation to form.

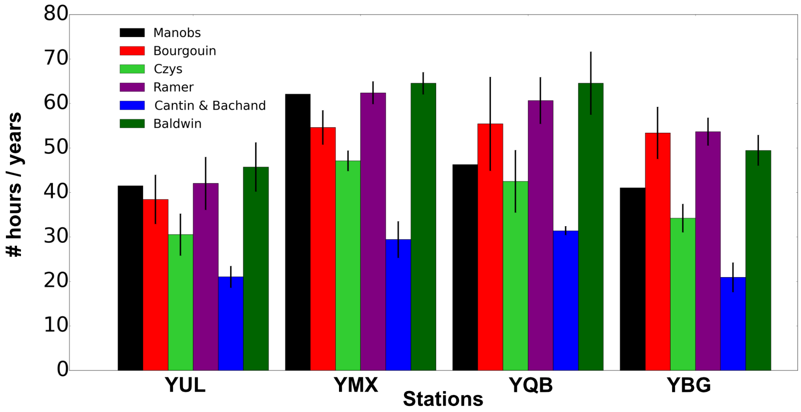

Fig. 3 Mean annual hourly occurrence of mixed precipitation of the observation, and diagnosed by Bourgouin, Czys, Ramer, CB, and Baldwin, for the locations of YMX, YUL, YQB and YBG, respectively. The black lines represent the standard deviation of the nine grid points nearest to the corresponding MANOBS stations.

The frequency distribution of events duration at Dorval, Québec (YUL) is shown in Fig. 4. The distribution for events with duration between 1 and 10 h shown in Fig.4a. In general, the observation and most of the algorithms reveal that the shortest duration events are the most frequent and the number of events decreases monotonically as their duration increases. The Ramer and the Czys algorithms overestimated the occurrence of 1-h events by around 12 and 20 events, respectively. But the large standard deviation of the nearest grid point suggests a sensibility in the chosen grid point for such short duration. The CB scheme, however, produced a flat distribution for the shortest duration events, and it underestimated the events that last less than 6h. For example, for the events lasting from 1 to 5 h, the occurrences are underestimated by 78, 68, 54, 58 and 63%, respectively. This underestimation correlates with the mean annual number of hours diagnosed by that method (Fig.2c and the blue color of Fig.3).

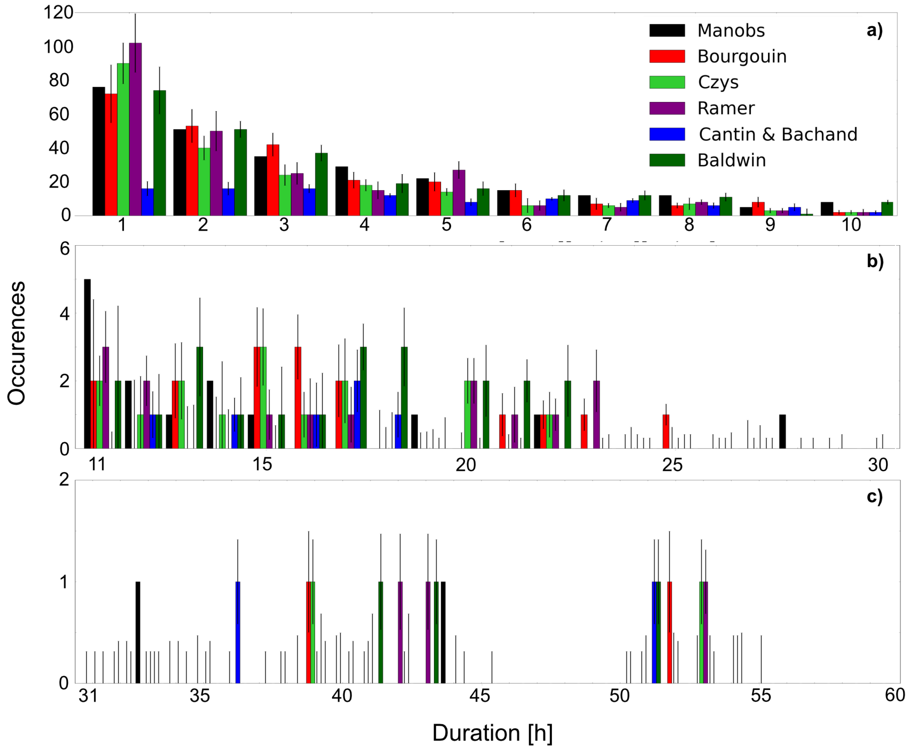

Fig. 4 Histograms of the number of hours per mixed precipitation events in different time ranges; (a) from 1 to 10 hours; (b) 11 to 30 hours and (c) 31 to 60 hours, for Dorval (YUL, Figure 1) for the 5 algorithms: Bourgouin, Czys, Ramer, CB, and Baldwin. The black lines represent the standard deviation of the nine grid points nearest to the MANOBS station.

The number of events with a duration from 11 to 30 h and from 31 h to 60 h are shown in Fig.4b and c, respectively. Those long-duration events are less frequent. For example, less than five events for duration between 11 and 30 h, and 1 event of duration between 31 and 60 h, although they vary among algorithms. This is due to the difficulty of the model to diagnose the duration of the events. For example, the observation may report an 11-h duration event when the model did not capture it because of no precipitation or/and no production of a melting/refreezing layer. Observational errors are also possible. Furthermore, the algorithms can diagnose different duration events. That being said, all algorithms diagnosed long-duration event meaning that the model correctly reproduced the long-duration atmospheric conditions associated with those events, which are discussed in the next subsection. In summary, similar statements can be made for the other stations. It is worth mentioning that the large standard deviation of the nine nearest grid point shows that the distribution is quite sensitive to the chosen grid point.

3.2 Atmospheric conditions associated with long- and short-duration events

To study the atmospheric conditions in which mixed precipitation events occur, short- ($<$6h) and long- ($\geq$6 h) duration events have been analyzed separately. Long-duration events are important because of the potential for severe conditions resulting from large accumulations despite the fact that freezing rain events are usually associated with light precipitation (Ressler et al., 2012).

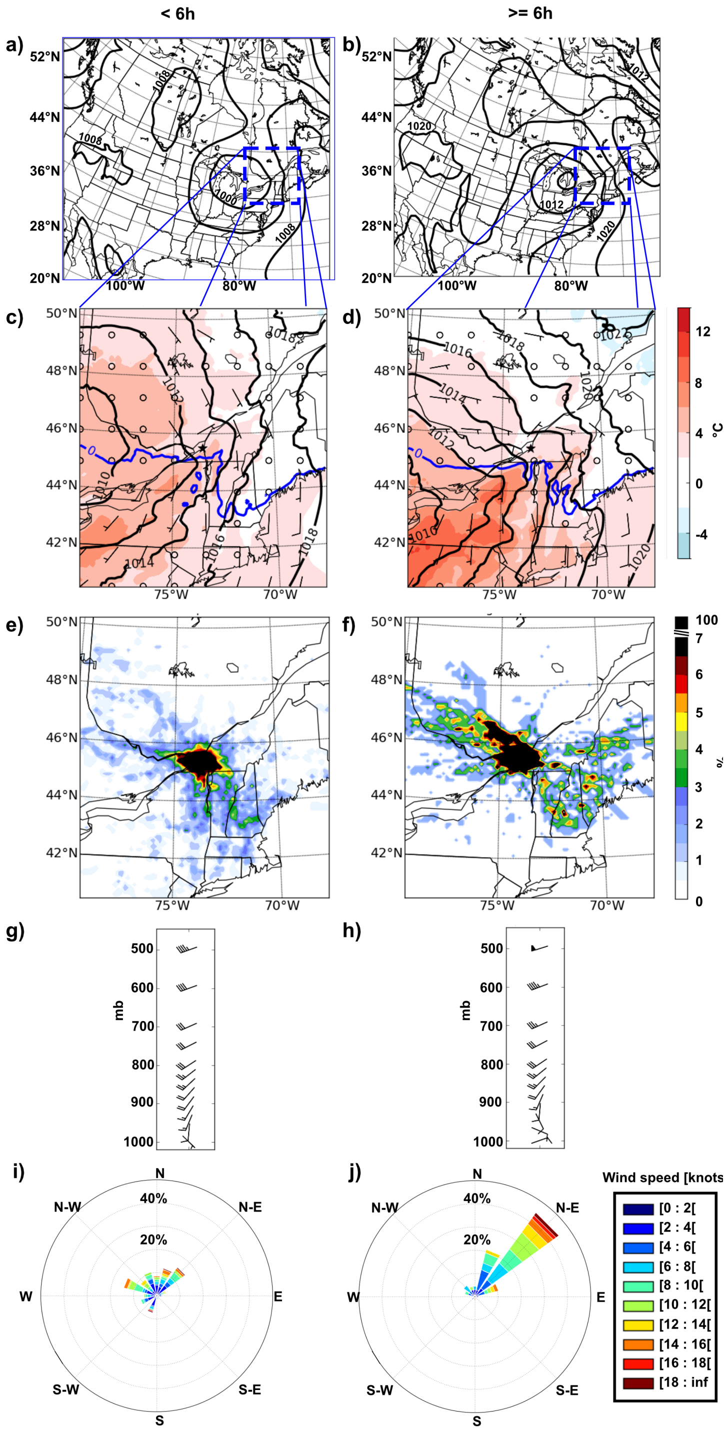

Fig. 5 Composite analysis at the beginning of all short-duration (left column) and long-duration (right column) mixed precipitation events. (a,b) show the mean sea level pressure (MSLP) in ERA-Interim, (c,d) show the simulated monthly 2-m temperature anomalies (color shading), the MSLP (black lines) and the 10-m wind speed and direction (barbs). The blue line is the 2-m 0°C isotherm. (e,f) show the frequencies (%) of mixed precipitation when occurring at YUL, (g,h) show the vertical profile of horizontal wind speed and direction at YUL, and (i,j) show the 10-m wind roses, with the colors indicating wind speed. The black star on the maps indicates the location of Dorval, Québec (YUL).

The synoptic scale pattern of the mean sea level pressure (MSLP) has been compiled for both short- and long-duration events (Fig.5a,b,c and d). Figure 5a-b show composites of the ERA-Interim MSLP at the nearest time associated with the beginning of events observed at YUL. The composite MSLP patterns are similar for short- and long-duration events, with a low pressure centered over Lake Huron and a ridge of high pressure over the Gaspé Peninsula. The pressure gradient over the SLRV, however, is much higher during the long-duration events. Figures 5c-d show composites of the monthly 2-m temperature anomalies, 2-meter 0°C isotherm, MSLP and 10-meter winds simulated by CRCM5 at the beginning of the mixed precipitation events diagnosed at YUL with the Bourgouin method. For both types of event, there is an area of cold air extending from the northeast to the southwest, as well as a gradient of MSLP in the SLRV. This pattern is much stronger for the long-duration events. These suggest warm air advection aloft (Cortinas Jr et al., 2004).

Figure 5e and f show maps of the frequency (%) of occurrence of mixed precipitation over the domain of interest at the beginning of events diagnosed at YUL. The patterns indicate a localized nature of the phenomenon, with the region of high frequency extending to more than 50-100 km farther from YUL for both types of event. For the long-duration events, however, an elongated north-west to south-east region of modest frequency is clear and could be associated with warm frontal passages (Cortinas, 2000). Warm air advection is confirmed by the wind veering during both types of events (Fig.5g-h), although much stronger for the long-duration events. Finally, a northeasterly 10-m wind (Fig.5i-j) is dominant at the beginning of the long-duration events, which supports the surface-based cold layer needed to produce mixed precipitation. No predominant wind direction is noted at the beginning of the short-duration events.

In summary, the MSLP and temperature anomaly patterns are similar for both types of event with a stronger signal associated with the long-duration ones. Northeasterly winds are predominant and stronger for the long-duration events. These provide favorable conditions to maintain the cold layer near the surface that is necessary for freezing rain.

3.3 Seasonal variation

Figure 6 shows the monthly number of hours and number of short- and long-duration events at 4 locations (YUL, YMX, YQB and YBG) indicated on Fig.1b. There is a maximum in both December and March. Although that fewer long-duration events occurred, they are responsible for a large proportion of annual mixed precipitation.

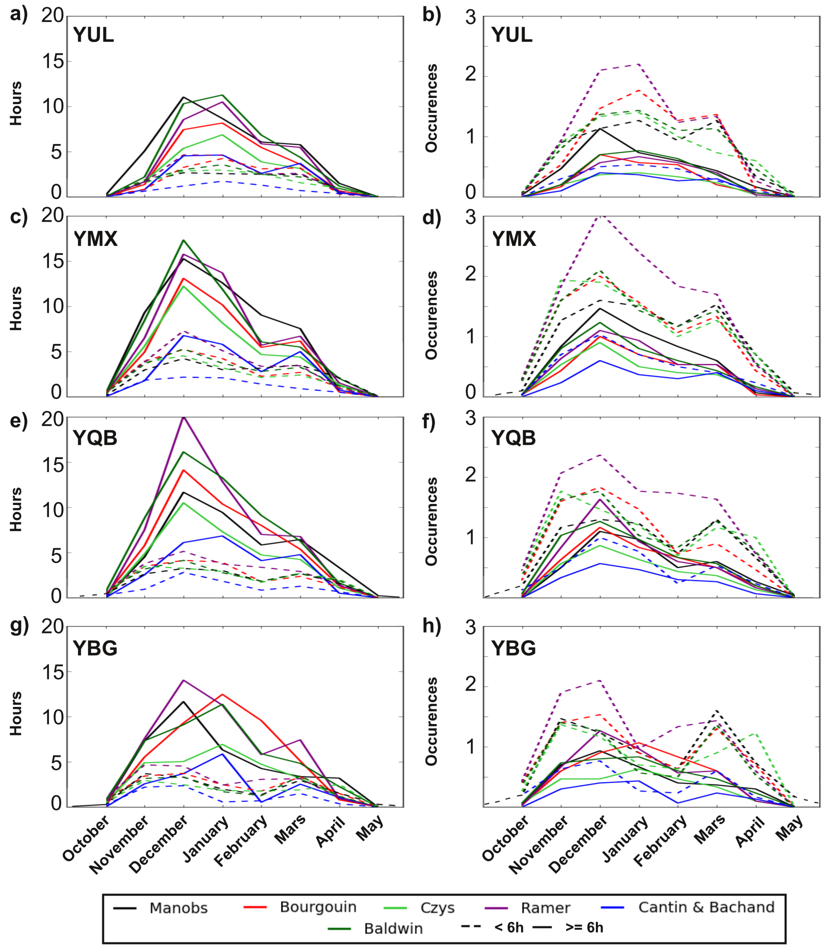

Fig. 6 Monthly number of hours (left column) and the number of events (right column) for (a,b) YUL, (c,d) YMX, (e,f) YQB and (g,h) YBG. The black lines correspond to the observed values while the colored lines correspond to the mixed precipitation diagnosed by the various algorithms, Bourgouin, Czys, Ramer, CB and Baldwin. The dashed lines and the plain lines are the short- and long-duration events, respectively.

4 Projected climate change of mixed precipitation

In this section, the climate changes (i.e. future - past) of mixed precipitation projected by CRCM5/MPI was analyzed. An additional analysis (Appendix A) shown that the historical simulation reproduced well the overall results from the hindcast simulation. Only differences with statistical significance greater of 95% (using a Wilcoxon rank-sum test) are shown.

The mean of the 5 algorithms for the past, future and climate change for the mean annual number of hours and the number of occurrences of short-duration events are given in Fig.7. The pattern of the future number of hours (Fig.7c) is comparable to the past (Fig.7a), but the number is reduced to the south and slightly increased to the north. Such a south to north migration of the number of annual hours of mixed precipitation follows the migration of the 0°C isotherm (not shown). The climate change (Fig.7e) indicates a small decrease of mixed precipitation in the SLRV near YUL, YMS and YQB. Figure 7f shows that the change in number of events follows a similar pattern as the change in the number of hours. In the SLRV the change correlated with the topography (not shown) while correlated less over the remaining of the domain.

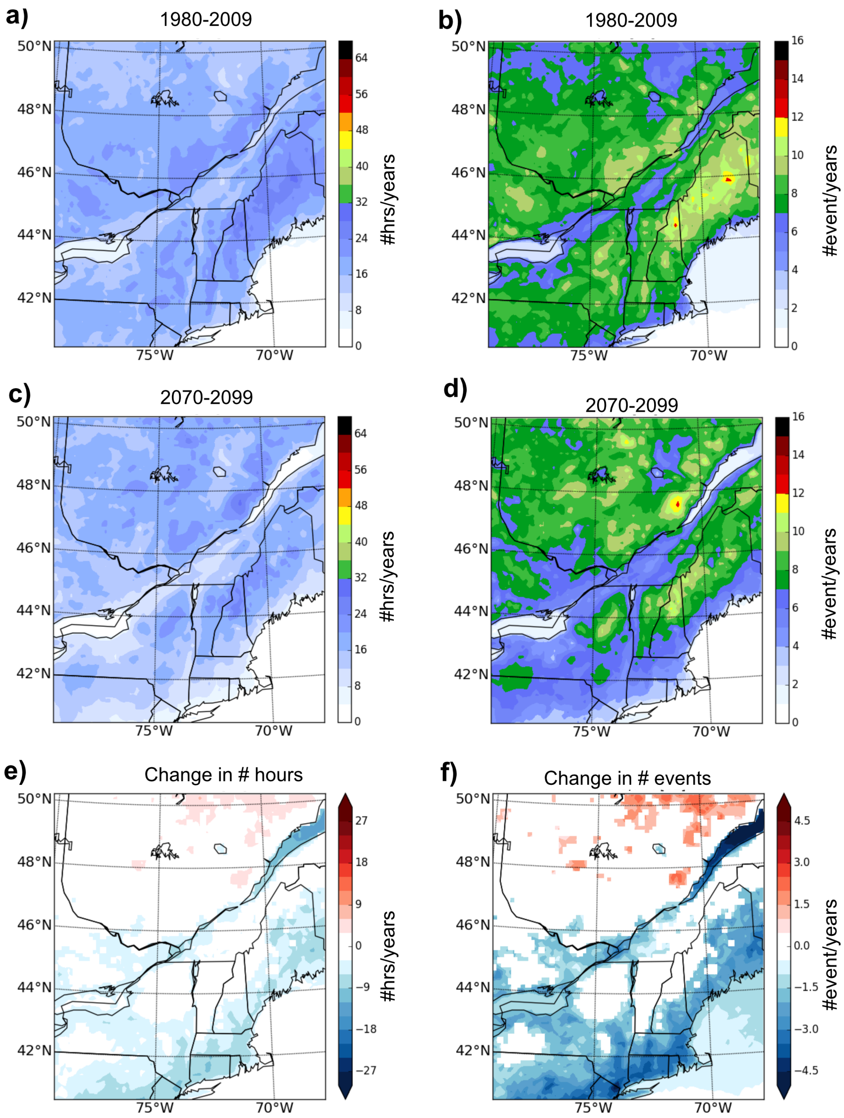

Fig. 7 Annual number of hours (left column) and the number of events (right column) for the period of (a,b) 1980-2009, (c,d) the period of 2070-2099, and (e,f) the corresponding changes for short-duration events the average of the 5 algorithms.

For the long-duration events, Fig.8 suggests a projected reduction of the mean number of hours and the number of events, but no clear northward migration of mixed precipitation in the future.

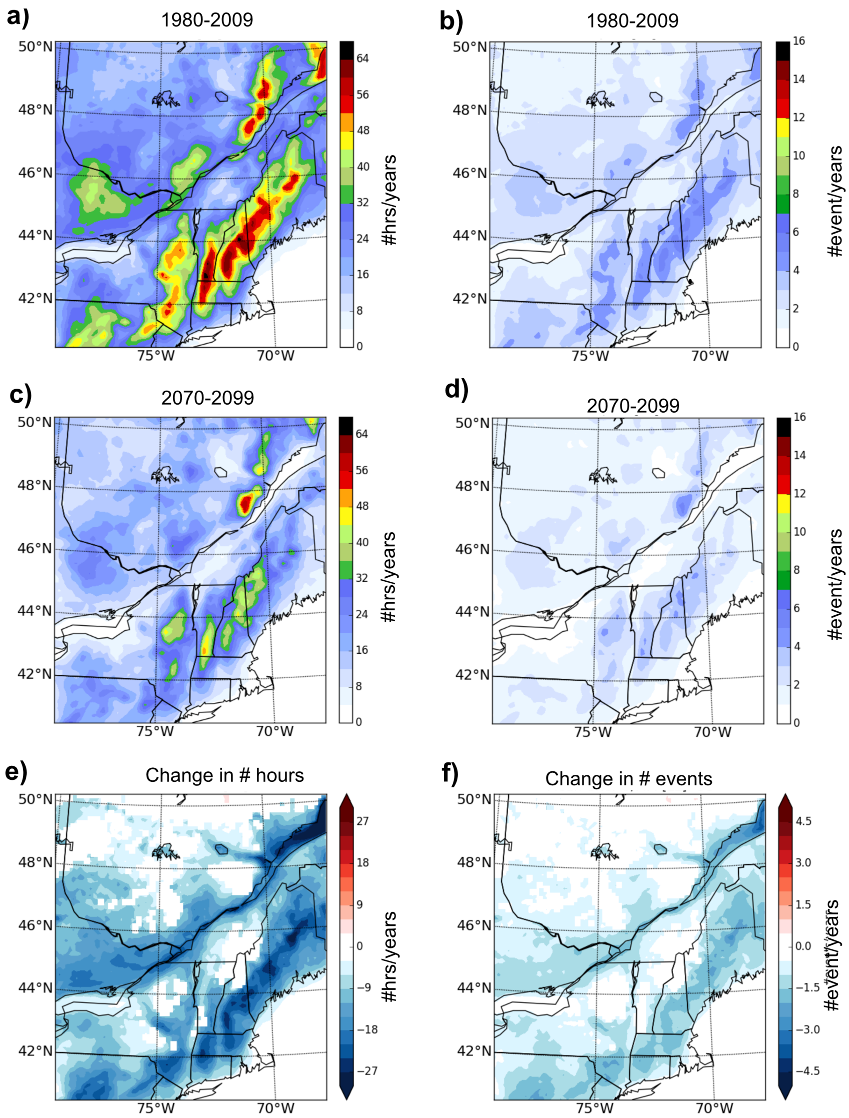

Fig. 8 Same as Fig.7, but for long-duration events

The climate-change projected number of hours and the number of short- and long-duration events per month at YUL, YMX, YQB and YBG are shown in Fig.9. The changes of the number of hours (Fig.9a-c-e-g) are different for short- and long-duration events. Small changes are suggested for short-duration events (generally less than 4 h) in the future, whereas the long-duration events are projected to decrease by down to 12 h. The maximum difference would occur between December and April depending on the location and the precipitation-typing algorithm. The average of all precipitation-typing algorithms suggest that the maximum decrease in occurrences occurs during the month of maximum occurrences identified in the historical simulation (not shown).

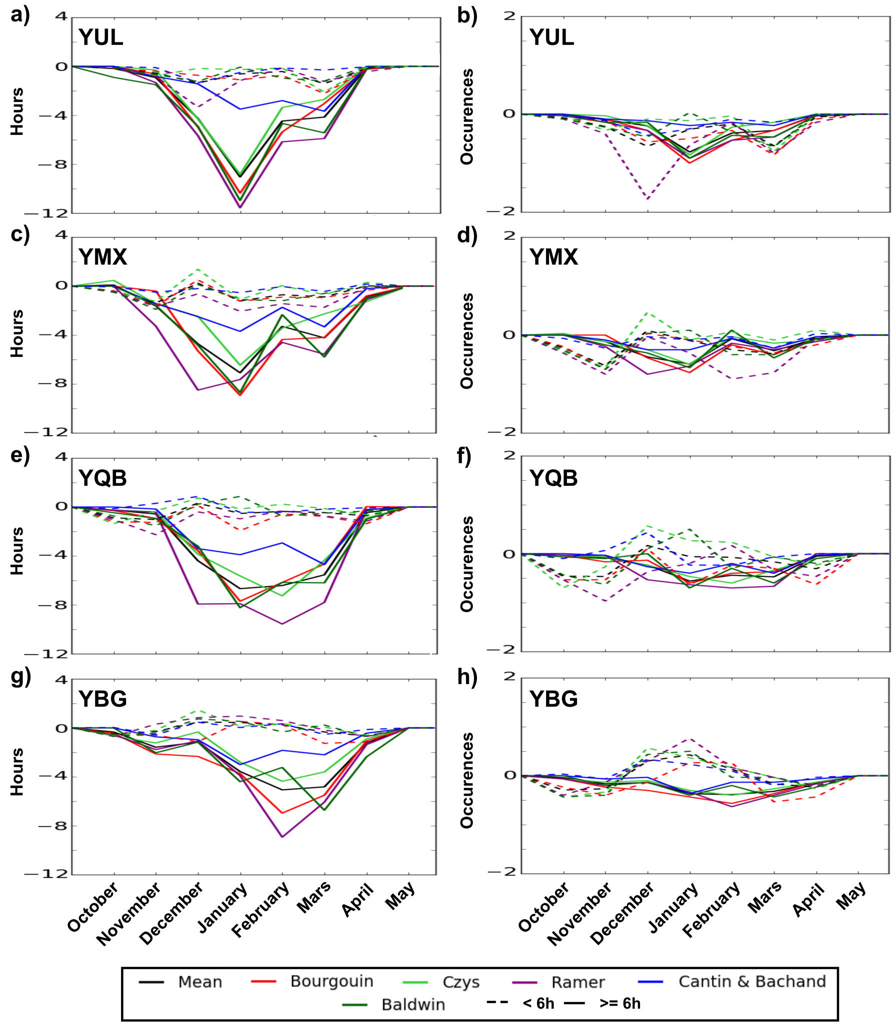

Fig. 9 Climate change of monthly hours (left column) and number of events (right column) of mixed precipitation at (a,b) YUL, (c,d) YMX, (e,f) YQB and (g,h) YBG as diagnosed by Bourgouin, Czys, Ramer, CB, and the average of the 5 algorithms.

The projected changes in the number of long-duration events (Fig.9b-d-f-h) are small at most locations, with the largest decrease occurring in January at YUL and YMX. The number of short-duration events will generally increase in December but decrease in fall (October, November), as well as at the end of the winter and early spring (February, March and April) at all locations except at YUL where all algorithms project a decrease. The general changes for short-duration events are probably due to the warmer temperatures that produced more favorable conditions for freezing rain during the winter, but less favourable conditions during the transition seasons.

5 Conclusions

This study focused on the occurrences of mixed precipitation (i.e. freezing rain and/or ice pellets) and its changes in the future over southern Québec. The fifth-generation Canadian Regional Climate Model has been used to downscale the Era-Interim reanalysis for hindcast and a simulation of the Max-Planck Institute (MPI) for Meteorology Earth System Model for the historical 1980-2009 and future 2070-2099 periods. Mixed precipitation has been diagnosed by post-processing the CRCM5 simulation using five algorithms. Short ($<$6h) and long ($\geq$6h) duration events have been analyzed separately to characterize their associated atmospheric conditions. For comparison with the observations, the closest grid point associated with a similar topographic height has been used when the occurrence of precipitation is compared at specific stations. But there is a great variability amongst the nearest grid points, which is discussed in Appendix B.

The climatology of the hindcast simulation has been studied using five diagnostic algorithms and the results were found to agree reasonably well with the observations. The algorithms captured the main pattern of mixed-precipitation occurrences, with some differences in the annual number of hours. The Bourgouin, the Czys, the Ramer and the Baldwin algorithms captured the relative maximum in the SLRV whereas partial thickness method of CB did not capture it. This is probably because this method compares the mean temperature of a layer, which cannot capture the shallow sub-freezing layer adequately near the surface during the short-duration events (<6h).

The combination of the surface pressure gradient and the temperature advection suggested that mixed precipitation generally occurs during a passage of a warm front. The high occurrence of northeasterly wind in the SLRV suggested that the long-duration events are maintained by the low-level cold air advection as discussed by Roebber and Gyakum (2003). It has also been shown that there are two maxima of occurrences, a main one in December and a second one in March, for both types of events. Although that the long-duration events are rare, they are responsible for the largest number of hours of mixed precipitation.

Finally, the projected changes indicated a poleward migration of the mixed precipitation occurrences, and a general reduction of long-duration events, both in their number of hours and in their number of occurrences.

Despite the benefits of using high-resolution climate simulations to realize a climate-change study of mixed precipitation, there remain numerous sources of modeling errors, such as the use of empirical diagnostic algorithms to discriminate precipitation types, the parameterization of subgrid-scale physical effects, internal structure of the model, imperfections in boundary conditions that drive the regional model, and the nesting technique. The low spatial density of observational datasets and the limited information about the precipitation types and intensity makes difficult the objective evaluation of simulated results. If diagnostic precipitation-type algorithms were to continue being used, they should at least be adjusted to optimize their performance for the region where they are applied. For example, drier climate conditions may need a different algorithm compared to a maritime moist climate. Eventually the diagnostic approach should be replaced by a physically based representation using detailed cloud and precipitation microphysical algorithm when computing resources allow it. An actionable assessment of projected changes of mixed precipitation would require using an ensemble of models and simulations to estimate the associated uncertainty.

This study takes place in an international endeavor to better understand climate using high-resolution climate simulations. To our knowledge, no study has investigated future mixed precipitation occurrence using such high spatial resolution. Although that our study brings a more detailed spatial and temporal description of this type of precipitation, further effort is needed to improve physically based representation of such precipitation types into climate models.

A Historical Simulation

To analyze the impact of the boundary conditions errors on the CRCM5 simulation, this section compares the CRCM5/ERA and the CRCM5/MPI simulations. Figure A1 shows the number of hours per year of occurrence of mixed precipitation for the average of the 5 algorithms, for the short- and long-duration events, in the hindcast and historical CRCM5 simulations, and their differences. Overall the differences in mixed precipitation are small. There is a slight positive bias south of the domain, which is more pronounced for the long-duration events mainly from December to February (not shown).

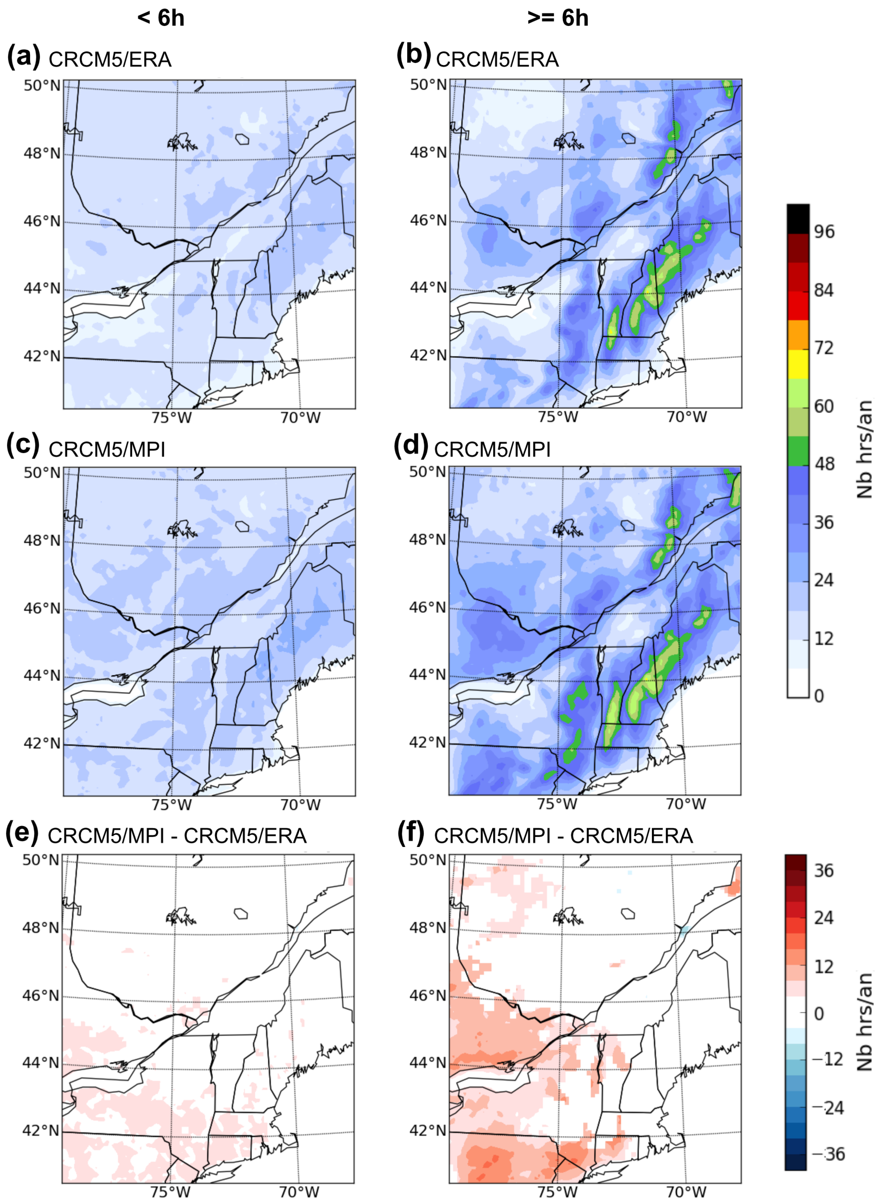

Fig. A1 Number of hours per year for short-duration events (left column) and long-duration events (right column) the average of the 5 algorithms in the reanalysis-driven hindcast simulation (a,b) CRCM5/ERA, MPI-ESM-LR-driven historical simulation (c,d) CRCM5/MPI, and (e,f) their difference.

Figure A2 shows the corresponding results for the number of events. The short-duration events show a positive bias in the south of the domain, with a maximum bias of 3 events per year. This positive bias in the number of events does not, however, have a strong impact on the number of hours, as noted in Fig.A1. On the other hand it is worth noting that the maximum occurrence of mixed precipitation happens in January in the historical simulation rather than in December as in the hindcast simulation (not shown). This shift in the maximum results from a warm bias of low atmospherics layers in the historical simulation driven by the MPI-ESM-LR.

Overall, the historical simulation is reproducing fairly the mixed precipitation climatology, which increases the confidant with the climate projection.

B Spatial variability

To compare the occurrence of mixed precipitation diagnosed in model simulations with observations, the closest grid point with similar topographic height has been used throughout this study. Several alternative options were also studied. A paramount finding was that there is a large variability amongst the adjacent model grid points for mixed precipitation. Figure B1 shows the simulated results and the observed values for short- and long-duration events. The range of values of the nine nearest grid points to the station reflects the spatial variability of adjacent grid points. Because mixed precipitation is sensitive to the surface elevation and the vertical atmospheric profile, this indicates that it may be inappropriate for such variable to use a spatial means of adjacent grid points to compare with observations. Comparing a simulation with observations

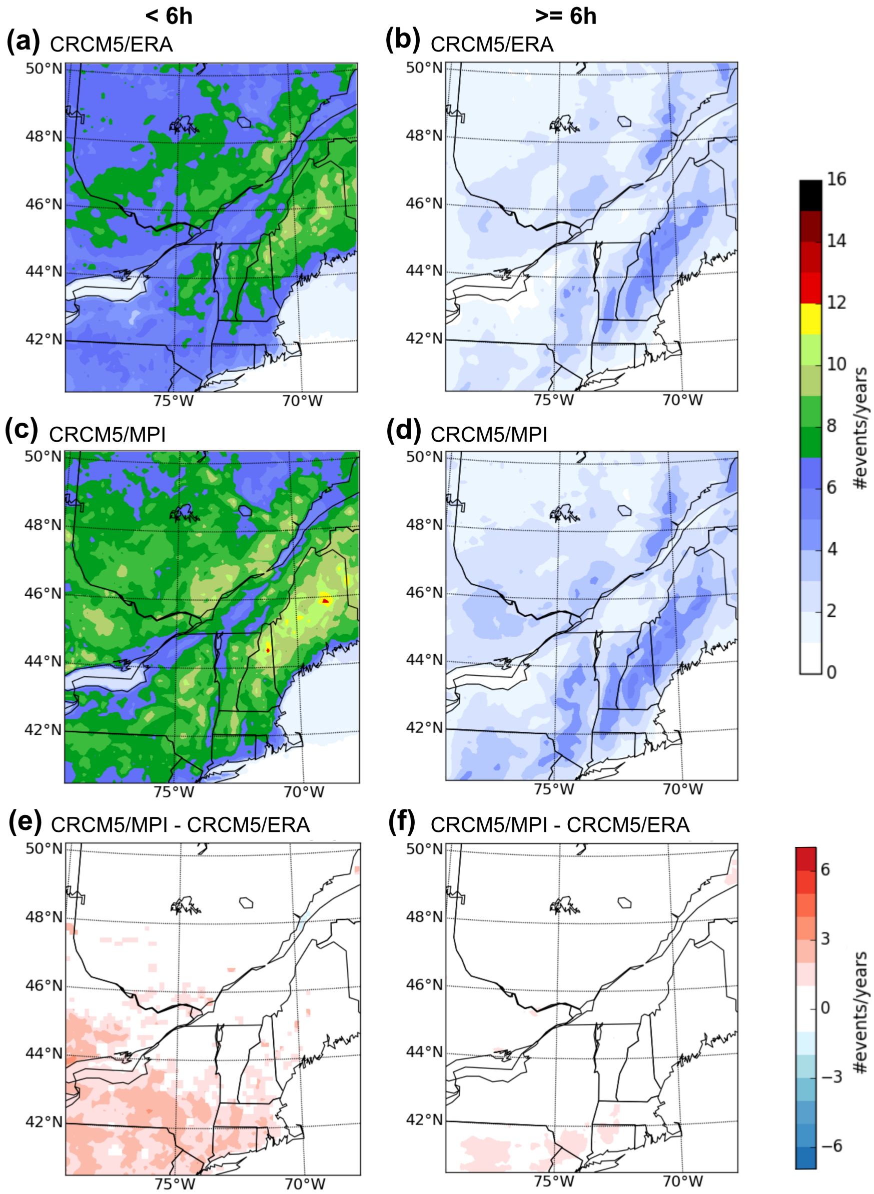

Fig. A2 Number of events per year for short-duration events (left column) and long-duration events (right column) the average of the 5 algorithms. in the reanalysis-driven hindcast simulation (a,b) CRCM5/ERA, MPI-ESM-LR-driven historical simulation (c,d) CRCM5/MPI, and (e,f) their difference.

is always challenging, and the task appears to be particularly difficult for mixed precipitation. In Fig.B1 it would be expected that observations are located within the range of the model results.

Acknowledgements This research was supported by 2 Discovery Grants of the Natural Sciences and Engineering Research Council (NSERC) of Canada. Computations were made on the supercomputer guillimin, managed by Calcul Québec and Compute Canada. The operation of this supercomputer is funded by the Canada Foundation for Innovation (CFI), the Fonds de recherche du Québec - Nature et technologies (FRQNT), NanoQuébec, and the Réseau de médecine génétique appliquée (RMGA). D.M. thanks the FRQNT for a graduate fellowship. The authors are greatly indebted to Dr. Émilie Bresson for her processing of the MANOBS and Eva Mekis to have provided them, to Dr. Bernard Dugas and Ms. Katja Winger for their essential help with the use of CRCM5, and to Mr. Georges Huard and Ms. Nadjet Labassi for maintaining user-friendly local computing facilities.

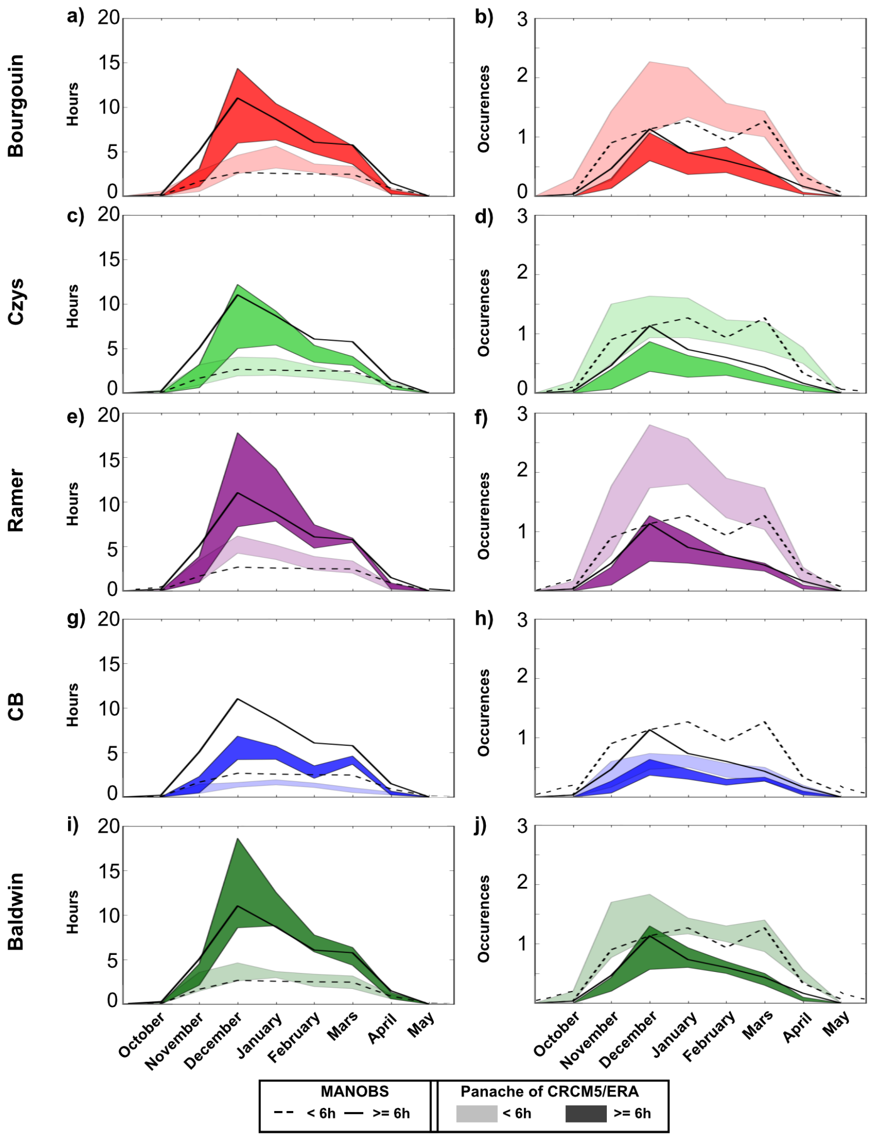

Fig. B1 Monthly number of hours (left column) and the number of events (right column) for YUL as diagnosed by Bourgouin (a,b), Czys (c,d), Ramer (e,f), CB (g,h) and Baldwin (i,j) from the hindcast CRCM5/ERA solution. The shaded area indicates the lowest and the highest values at the nine grid points nearest to the YUL station. The black lines and the dark colors correspond to the observed value and the simulated results, respectively, for the long-duration events. The dashed lines and the pale colors are the observed value and the simulated results, respectively, for the short-duration events.

References

Baldwin E, Contorno S (1993) Development of a weather-type prediction system for NMC's mesoscale ETA model. In: Preprints, 13th Conf. on Weather Analysis and Forecasting, Vienna, VA, Amer. Meteor. Soc, pp 86–87

Bélair S, Mailhot J, Girard C, Vaillancourt P (2005) Boundary layer and shallow cumulus clouds in a medium-range forecast of a large-scale weather system. Mon Weather Rev 133(7):1938–1960

Bélair S, Roch M, Leduc AM, Vaillancourt PA, Laroche S, Mailhot J (2009) Medium-range quantitative precipitation forecasts from Canada's new 33-km deterministic global operational system. Weather Forecast 24(3):690–708

Benoit R, Côté J, Mailhot J (1989) Inclusion of a TKE boundary layer parameterization in the Canadian regional finite-element model. Mon Weather Rev 117(8):1726–1750

Bernstein BC (2000) Regional and local influences on freezing drizzle, freezing rain, and ice pellet events. Weather Forecast 15(5):485–508

Bourgouin P (2000) A method to determine precipitation types. Weather Forecast 15(5):583–592

Bresson E, Laprise R, Paquin D, Thériault J, de Elía R (2017) Evaluating the ability of CRCM5 to simulate mixed precipitation. Atmos-Ocean 55(2):79–93

Cantin A, Bachand D (1993) Synoptic pattern recognition and partial thickness techniques as a tool for precipitation types forecastng associated with a winter storm. Tech. rep., Environnement Canada, 9 p.

Carrera ML, Gyakum JR, Lin CA (2009) Observational study of wind channeling within the St. Lawrence river valley. J Appl Meteorol Clim 48(11):2341–2361, doi: 10.1175/2009JAMC2061.1

Cheng C, Auld H, Li G, Klaassen J, Li Q (2007) Possible impacts of climate change on freezing rain in south-central Canada using downscaled future climate scenarios. Nat Hazard Earth Sys 7(1):71–87

Cheng CS, Li G, Auld H (2011) Possible impacts of climate change on freezing rain using downscaled future climate scenarios: updated for eastern Canada. Atmos-Ocean 49(1):8–21

Cholette M, Laprise, Thériault JM (2015) Perspectives for very high-resolution climate simulations with nested models: Illustration of potential in simulating St. Lawrence River valley channelling winds with the fifth-generation Canadian Regional Climate Model. Climate 3(2):283–307, DOI 10.3390/cli3020283

Cortinas J (2000) A climatology of freezing rain in the great lakes region of North America. Mon Weather Rev 128(10):3574–3588

Cortinas J, Brill K, Baldwin M (2002) Probabilistic forecasts of precipitation type. In: Preprints, 16th Conf. on Probability and Statistics in the Atmospheric Sciences, Orlando, FL, Amer. Meteor. Soc, vol 3

Cortinas Jr JV, Bernstein BC, Robbins CC, Walter Strapp J (2004) An analysis of freezing rain, freezing drizzle, and ice pellets across the United States and Canada: 1976-90. Weather Forecast 19(2):377–390, doi: 10.1175/1520-0434(2004)019¡0377:AAOFRF¿2.0.CO;2

Czys RR, Scott RW, Tang K, Przybylinski RW, Sabones ME (1996) A physically based, nondimensional parameter for discriminating between locations of freezing rain and ice pellets. Weather Forecast 11(4):591–598

Delage Y, Girard C (1992) Stability functions correct at the free convection limit and consistent for both the surface and Ekman layers. Bound Layer Meteor 58(1-2):19–31

Delage YAA (1997) Parameterising sub-grid scale vertical transport in atmospheric models under statically stable conditions. Bound Layer Meteor 82(1):23–48

Drake J, Mason B (1966) The melting of small ice spheres and cones. Q J Roy Meteor Soc 92(394):500–509

Groisman PY, Bulygina ON, Yin X, Vose RS, Gulev SK, Hanssen-Bauer I, Førland E (2016) Recent changes in the frequency of freezing precipitation in North America and Northern Eurasia. Environ Res Lett 11(4):045,007–

Henson W, Stewart R, Kochtubajda B, Thériault J (2011) The 1998 ice storm: Local flow fields and linkages to precipitation. Atmos Res 101(4):852–862

Hernández-Díaz L, Laprise R, Sushama L, Martynov A, Winger K, Dugas B (2013) Climate simulation over CORDEX Africa domain using the fifth-generation Canadian Regional Climate Model (CRCM5). Clim Dyn 40(5-6):1415–1433, DOI 10.1007/s00382-012-1387-z,

Kain JS, Fritsch JM (1990) A one-dimensional entraining/detraining plume model and its application in convective parameterization. J Atmos Sci 47(23):2784–2802

Klima K, Morgan MG (2015) Ice storm frequencies in a warmer climate. Climatic Change 133(2):209–222

Kuo HL (1965) On formation and intensification of tropical cyclones through latent heat release by cumulus convection. J Atmos Sci 22(1):40–63

Lambert SJ, Hansen BK (2011) Simulated changes in the freezing rain climatology of north america under global warming using a coupled climate model. Atmos-Ocean 49(3):289–295

Li J, Barker HW (2005) A radiation algorithm with correlated-k distribution. Part I: local thermal equilibrium. J Atmos Sci 62(2):286–309

Lucas-Picher P, Laprise R, Winger K (2016) Evidence of added value in North American regional climate model hindcast simulations using ever-increasing horizontal resolutions. Clim Dyn pp 1–23

Martynov A, Sushama L, Laprise R, Winger K, Dugas B (2012) Interactive lakes in the Canadian Regional Climate Model, version 5: the role of lakes in the regional climate of North America. Tellus A 64, DOI 10.3402/tellusa.v64i0.16226

Matte D, Laprise R, Thériault JM (2016) Comparison between high-resolution climate simulations using single- and double-nesting approaches within the Big-Brother experimental protocol. Clim Dyn 47(12):3613–3626, DOI 10.1007/s00382-016-3031-9

Matte D, Laprise R, Thériault JM, Lucas-Picher P (2017) Spatial spin-up of fine scales in a regional climate model simulation driven by low-resolution boundary conditions. Clim Dyn 49(1-2):563–574, URL http://dx.doi.org/10.1007/s00382-016-3358-2

McFarlane NA (1987) The effect of orographically excited gravity wave drag on the general circulation of the lower stratosphere and troposphere. J Atmos Sci 44(14):1775–1800

Meinshausen M, Smith SJ, Calvin K, Daniel JS, Kainuma M, Lamarque J, Matsumoto K, Montzka S, Raper S, Riahi K (2011) The RCP greenhouse gas concentrations and their extensions from 1765 to 2300. Climatic change 109(1-2):213–241

Milbrandt JA, Yau MK (2005a) A multimoment bulk microphysics parameterization. Part I: Analysis of the role of the spectral shape parameter. J Atmos Sci 62(9):3051–3064

Milbrandt JA, Yau MK (2005b) A multimoment bulk microphysics parameterization. Part II: A proposed three-moment closure and scheme description. J Atmos Sci 62(9):3065–3081

Morrison H, Grabowski WW (2008) A novel approach for representing ice microphysics in models: Description and tests using a kinematic framework. J Atmos Sci 65(5):1528–1548

Morrison H, Milbrandt JA (2015) Parameterization of cloud microphysics based on the prediction of bulk ice particle properties. Part I: Scheme description and idealized tests. J Atmos Sci 72(1):287–311

Rackley JA, Knox JA (2016) A climatology of southern appalachian cold-air damming. Weather Forecast 31(2):419–432

Ramer J (1993) An empirical technique for diagnosing precipitation type from model output. In: Amer. Meteor. Soc., International conference on aviation Weather Systems, 5th, Vienna, VA, pp 227–230

Reeves HD, Elmore KL, Ryzhkov A, Schuur T, Krause J (2014) Sources of uncertainty in precipitation-type forecasting. Weather Forecast 29(4):936–953

Ressler GM, Milrad SM, Atallah EH, Gyakum JR (2012) Synoptic-scale analysis of freezing rain events in Montreal, Quebec, Canada. Weather Forecast 27(2):362–378

Roebber PJ, Gyakum JR (2003) Orographic influences on the mesoscale structure of the 1998 ice storm. Mon Weather Rev 131(1):27–50

Stuart RA, Isaac GA (1999) Freezing precipitation in Canada. Atmos-Ocean 37(1):87–102

Sundqvist H, Berge E, Kristjánsson JE (1989) Condensation and cloud parameterization studies with a mesoscale numerical weather prediction model. Mon Weather Rev 117(8):1641–1657

Verseghy DL (2000) The Canadian land surface scheme (CLASS): its history and future. Atmos Ocean 38(1):1–13

Verseghy L (2008) The Canadian land surface scheme: technical documentation–version 3.4. Climate Research Division, Science and Technology Branch, Environment Canada

Whiteman CD, Doran JC (1993) The relationship between overlying synoptic-scale flows and winds within a valley. J Appl Meteorol 32(11):1669–1682

Zadra A, Roch M, Laroche S, Charron M (2003) The subgridscale orographic blocking parametrization of the GEM model. Atmos-Ocean 41(2):155–170